Materials Today Chemistry 26 (2022) 101240

Contents lists available at ScienceDirect

Materials Today Chemistry

journal homepage: www.journals.elsevier.com/materials-today-chemistry/

Supercritical carbon dioxide assisted synthesis of ultra-stable sulfur/carbon composite cathodes for Li– S batteries

L.S. Shankar [a], D. Zalka [a, b, c], T. Szabó [d], E. Székely [f], M. Kőrösi [f], Z. Pászti [a], K. Balázsi [e], L. Illés [e], Z. Czigány [e], R. Kun [a, f, *]

[a] Institute of Materials and Environmental Chemistry, Research Centre for Natural Sciences, H-1117 Budapest, Magyar Tudósok Krt. 2, Budapest, Hungary
[b] Institute of Materials Research, Slovak Academy of Sciences, Watsonova 47, 04001 Košice, Slovak Republic
[c] Faculty of Science, Institute of Physics, Pavol Jozef Šafárik University in Košice, Košice 041 80, Slovak Republic
[d] Department of Physical Chemistry and Materials Science, University of Szeged, Rerrich Béla Tér 1, Szeged, 6720, Hungary
[e] Institute of Technical Physics and Materials Science, Center for Energy Research, Konkoly Thege Miklós út 29-33, H-1121 Budapest, Hungary
[f] Department of Chemical and Environmental Process Engineering, Faculty of Chemical Technology and Biotechnology, Budapest University of Technology and Economics, Műegyetem Rkp. 3, H-1111 Budapest, Hungary

ARTICLE INFO

Article history:
Received 10 August 2022
Received in revised form
23 September 2022
Accepted 5 October 2022
Available online xxx

Keywords:
Li–S battery
Sulfur cathode
Carbon–sulfur composite
Reduced graphene oxide
Supercritical fluid
Polysulfide confinement

ABSTRACT

To mitigate the shuttle effect and enhance the electrical conductivity in lithium battery cathode, the unique characteristics of supercritical CO_2 solvent (SC–CO_2) and the distinctive porous and layered microstructure of reduced graphene oxide (rGO) are exploited in the fabrication of a high-performance rGO/sulfur composite cathode. Exploiting SC-CO_2 technology can realize highly efficient sulfur transfer and precise microstructure regulation of S/C composite cathodes for Li–S batteries. On exposure, due to the sudden pressure release process, the SC-CO_2 expands the interlayers of rGO rendering plenty of storage space for small sulfur allotropes in carbon matrices which increases the active sulfur loading. Being a remarkable hydrophobic solvent, the wetting properties of SC-CO_2 are excellent, ensuring sulfur dissolution and penetration deep into the voids and interlayers of rGO. This creates intimate contact of sulfur with rGO interlayers, guaranteeing precise sulfur content, uniform sulfur distribution, and strong interaction between sulfur and carbon leading to enhanced electrical conductivity and sulfur utilization efficiency. Another important feature is that the S/C composites can be prepared at room temperature, unlike other conventional techniques which require a higher temperature. Moreover, the product mixture can be separated simply by de-pressuring SC-CO_2. Herein, the rGO/sulfur composite cathode prepared on a lab scale showed an initial discharge capacity of 1024 mAh/g at 0.1C rate with capacity retention of 92.2% and coulombic efficiency of 99% even after 200 charge-discharge cycles. The developed cells showed excellent performance (929 mAh/g at 1 C rate) with an ultralow decay of 0.04% per cycle even after 200 charge-discharge cycles. Through this work, we believe that the synergistic effect of SC-CO_2 technology and rGO as sulfur host will open up a promising future for the synthesis of efficient S/C composite cathodes with ultra-high cycling stability.

1. Introduction

Growing population, advancing economies, and changing lifestyles are all leading to one factor: ever-increasing energy demands of the mankind. As energy usage increases, concerns about environmental pollution associated with the use of fossil fuels are becoming serious. To mitigate these issues and reduce our dependence on fossil fuels, alternative energy technologies based on renewable sources like solar and wind energies need to be developed and adopted. However, these energy sources are intermittent and lack consistency [1]. When it comes to storing electrical energy, rechargeable batteries still stand at the top of the list because of their cost-effectiveness and numerous other advantages. Li-ion batteries have become prominent over the past two decades, particularly for portable electronics, as they offer a much higher energy density than other rechargeable systems. The current Li-ion technology is driven by the insertion-compound anode and cathode materials, which are in turn known for their limitations in

* Corresponding author.
E-mail address: kun.robert@ttk.hu (R. Kun).

https://doi.org/10.1016/j.mtchem.2022.101240

terms of charge-storage capacity and energy density. To overcome the charge-storage limitations of the insertion-compound electrode, materials that undergo conversion reactions while accommodating more ions and electrons are becoming a promising option but are highly challenging. In this perspective, the Li–S batteries with high energy density are being intensively pursued.

Sulfur, one of the most abundant elements of the Earth's crust benefiting from profitability and non-toxicity, is highly attractive as a cathodic material. It has a high theoretical capacity of 1672 mAh/g, which is an order of magnitude superior to that of transition metal oxide cathodes. The conversion reaction of sulfur to form lithium sulfide (Li_2S) by reversibly incorporating two electrons per sulfur atom results in high capacity [2–17]. Despite these considerable advantages, there are still a few challenges to be tackled in developing stable, reversible, and efficient sulfur cathodes in Li–S batteries. One of the major concerns is that the conversion reaction is always accompanied by a large volume change. Additionally, sulfur and lithium sulfide are both insulators, which calls for the need for incorporating conductive additives like carbon into the electrodes [1]. Moreover, the intermediate lithium polysulfides formed during the conversion reaction are soluble in most of the liquid electrolytes used to date. These soluble intermediate Li polysulfides diffuse through the electrolyte to the Li anode and get reduced to form solid Li sulfide precipitates, passivating the anode by irreversible precipitation. This results in low active material utilization, low coulombic efficiency, and short cycle life for the sulfur cathode [1]. Although the Li–S batteries are believed to be one of the most promising next-generation high-energy-density rechargeable battery chemistries, the cycle life and efficiency need to be improved for them to be employed in practical applications.

One of the major challenges in developing efficient cathode materials is in finding suitable strategies to confine sulfur in carbon hosts with the required microstructure. When designing sulfur hosts for long-term stable operation and high energy density, an ideal host does not just need to have abundant porosity and large surface area, but also should possess high electronic conductivity. This may allow large confinements of active material, support fast electrochemical reaction kinetics and strongly interact with polysulfides [18].

Porous carbons play key roles in Li–S batteries due to their good conductivity, abundant porosity, and good electrochemical stability [19]. They possess good electrical conductivity, a large surface area, and tunable surface chemistry [20]. The well-defined porosity and functional groups can relieve the volume changes and meanwhile provide a strong affinity for polysulfides, which can retard the polysulfides shuttle and enable high stable cycling life [20,81]. Microporous carbon hosts can efficiently confine smaller sulfur particles in their pores rendering excellent cycle stability and better electrolyte compatibility, but they can only afford limited sulfur content, hindering their practical application. Mesoporous and macro porous carbon provides larger pore volumes to accommodate more sulfur rendering high areal sulfur loading and energy density of the battery. But, the challenge with large-sized sulfur particles confined in large pore channels is that they could restrict the electronic conductivity and the sulfur utilization rate. This limitation makes it necessary to take actions from the synthesis aspect to continuously regulate and optimize the microstructure and surface chemistry of carbon materials (such as pore size, surface area, morphology, conductive functional groups, etc.) to improve the dynamic properties and structural stability of the carbon-sulfur composite cathodes, and finally its capacity, safety, rate performance, cycle stability, and energy density [18]. During the past years, a variety of carbon materials with different morphologies and porous structures have been explored like hollow carbon spheres, porous activated carbons, carbon fibers, carbon nanotubes, carbon monoliths, graphene, etc. [6,21–28,81].

In addition to the importance of investigating various carbon materials, it is instructive to look at how various synthesis routes of carbon/sulfur composites influence the cell performance since a suitable sulfur encapsulation is a major key to improving the utilization of the active material and limiting the loss of the active material. To date, different strategies such as mechanical mixing, heat treatment, solution-based synthesis, etc. Have been exploited by the research community. This includes melt diffusion [29,30], solution infiltration [31,82], chemical vapor deposition [32,83], mechanical infusion such as ball milling [33], wet chemical processes utilizing soluble sulfur-containing compound (sodium thiosulfate, sodium sulfide, sodium polysulfide etc.) [8,34–37]. However, these methods involve the usage of toxic solvents like CS_2, benzene, toluene, etc., and demand high energy consumption. Moreover, a precise sulfur content with its uniform distribution and affinity with the carbon host cannot be guaranteed. In this regard, the development of a more facile, sustainable and efficient strategy is paramount for the synthesis of the high-performance sulfur cathode in Li–S batteries.

In this article, we report a simple, rapid, and green route allowing highly efficient impregnation of sulfur into carbon matrix using supercritical carbon dioxide (SC–CO_2) medium to fabricate Carbon-sulfur (S/C) composite cathode for Li–S batteries. Compared to the conventional synthesis techniques, the exploitation of SC-CO_2 with hybrid properties of “gas-like” (in terms of volume filling) and “liquid-like” (in terms of density and dissolving power), has received great attention in materials synthesis owing to its unparalleled merits. SC-CO_2 is a promising hydrophobic solvent that has the comparable dissolving ability of non-polar sulfur to that of the highly toxic carbon disulfide (CS_2), guaranteeing that sulfur can be effectively dissolved at the molecular level [38]. It possesses low viscosity, high diffusivity, and zero surface tension like gas as well as appreciable density and solvation power like a liquid, and its dissolving power can be adjusted by changing pressure and temperature [39]. While the liquid-like density and solvation power of modified SC-CO_2 allows for the dissolution of sulfur, its gas-like diffusivity and viscosity facilitate diffusion and permeation of dissolved sulfur into the depth of micropores and mesopores more rapidly and efficiently as compared to the conventional wet impregnation techniques employing toxic solvents. On exposure, due to the sudden pressure release process, the SC-CO_2 expands the interlayers of rGO rendering plenty of storage space for small sulfur allotropes in carbon matrices. This creates direct contact of sulfur with rGO interlayers, guaranteeing precise sulfur content, uniform sulfur distribution, and strong interaction between sulfur and carbon leading to enhanced electrical conductivity and sulfur utilization efficiency. Another important feature is that the product can be separated simply by depressuring of SC-CO_2. In addition, SC-CO_2 is non-toxic, non-flammable, cost-effective, and recyclable, and the liquid waste problem can also be minimized [40]. This strategy of utilizing SC-CO_2 by eliminating the toxic solvents for sulfur dissolution makes supercritical technology a “green process”.

In this work, SC-CO_2 technology, which has so far received little attention in battery studies, is utilized in encapsulating sulfur into a porous reduced graphene oxide host, and the feasibility of SC-CO_2 media to formulate S/C composite is evaluated. Herein, the graphene oxide is prepared by the modified Hummer's method [41,42]. GO consists of graphene sheets decorated mostly with epoxide and hydroxyl groups. But GO, like graphite oxide, is an electrical insulator, due to the disruption of its sp^2 bonding networks. Therefore, in this work, GO is reduced by heat treatment, producing reduced graphene oxide, rGO [43]. Reduced graphene

oxide possesses a special kind of layered, disordered microstructure providing more interlayer space, serving as a perfect host material that can enable the facile intercalation of active sulfur particles enabling faster reaction kinetics.

Employing the as-prepared rGO/sulfur composite cathode can realize the highly efficient intercalation/anchoring of sulfur within the rGO host and precise microstructure regulation of S/C composite cathodes for Li−S batteries. This ultimately helps diminishing the shuttle effect of lithium polysulfides, thereby enhancing the electrochemical stability in Li−S batteries.

2. Materials and methods

2.1. Synthesis of graphene oxide using modified Hummer's method

The most common chemical synthesis route for GO is Hummer's method and modified Hummer's method [41,42]. In this work, we have employed modified Hummer's method for the preparation of GO. This modified method of synthesis involves both oxidation and exfoliation of graphite sheets due to the thermal treatment of the solution. In this stepwise synthesis procedure, 2 g graphite powder (SGA-20, 99.9% carbon content) and 2 g $NaNO_3$ (Sigma Aldrich, 99%) were mixed in 60 ml of H_2SO_4 (Sigma Aldrich, 98%) in a 1000 ml flask with gentle, continuous stirring. Later 6 g of potassium permanganate (Sigma Aldrich, 99%) was added stepwise to the suspension. The rate of addition was carefully controlled to keep the reaction temperature lower than 15 °C.

The mixture was kept stirring for 2 h and was later diluted with 60 ml water placed above an ice bath. The solution was kept at ambient temperature until it was cooled down completely. The resulting mixture was then treated with H_2O_2 and the solution was changed to bright yellow. The resulting mixture was then washed by centrifugation with deionized water several times until it formed a thick gel-like brown suspension and a clear distinction between GO sedimentation and DI water was visible. In order to remove the impurities, this thick brown suspension was dialyzed for a few days. The GO after dialysis was freeze-dried overnight to yield the GO powder. Later this freeze-dried pristine GO was thermally reduced at 350 °C under a nitrogen atmosphere for 30 min to obtain reduced GO (rGO) for the SC-CO_2 assisted sulfur-containing composite formation.

2.2. Supercritical CO_2-assisted synthesis of rGO/sulfur composites

In the synthesis of carbon/sulfur composite, the as-prepared rGO and elemental sulfur powder were mixed in a mass ratio of 2:1 and transferred into the high-pressure supercritical reactor. Subsequently, CO_2 (99.9%) was pumped into the reactor and the mixture was agitated at 350 RPM for 12 h. The temperature and pressure during the whole process were maintained at 32 °C and 100 bars respectively. After the SC−CO_2−assisted milling, the reactor was gently depressurized by releasing out CO_2. The as-prepared rGO/sulfur composite powder was then collected from the reactor, hereby denoted as RGO-S-SCC. Additionally, to understand and compare the effects of post heat treatment of the composite prepared with the aid of supercritical CO_2 on the electrochemical performance of the cells, a small portion of the as-prepared sample was taken apart and heated at 250 °C for 20 min in a tubular furnace under nitrogen atmosphere, hereby denoted as RGO-S-SCC 250. For the comparative study, reference carbon/sulfur composite was made by conventional melt diffusion synthesis protocol. In this method, carbon black and sulfur are mixed well in mass ratio of 2:1, followed by heat treatment at 155 °C (5 °C/min) for 12 h under Ar atmosphere, in order to obtain S/C composite (hereby denoted as S/C Melt Diffusion).

2.3. Materials characterization

X-ray diffraction (XRD) patterns were obtained using PW3040/60 (Philips, Netherlands) X-ray diffractometer with a Cu-Ka radiation source ($\lambda = 1.5418$ Å; 40 kV acceleration voltage; Ni filter used as a beta-filter). The Raman spectra were recorded using a Raman microscope (BIOLAB) with Nd-YAG 1064 laser excitation in the range of 100−2000 cm^{-1}. The surface area was determined by the Brunauer−Emmett−Teller (BET) method based on nitrogen adsorption-desorption tests using Surfer advanced data processing (ThermoFisher Scientific). The pore volume is obtained under the assumption of the validity of the Gurvich rule. Thermogravimetric analysis was performed on Labsys Evo (SETARAM) under a flowing N_2 atmosphere with a heating rate of 10 °C/min from room temperature to 700 °C.

The morphology, microstructure and elemental distribution were observed using scanning electron microscopy (SEM, FEI Quanta 3D dual-beam equipment) and energy dispersive X-ray spectrometry (EDX) (EDAX Apollo SSD detector coupled with Genesis software). Lamellae of the samples were prepared by focused ion beam technique (FIB) using a ThermoFisher Scientific Scios 2 dual beam system. Two final polishing procedures were applied in FIB sample preparation: 5 kV and 48 pA and 2 kV 27 pA to minimize artefacts. TEM investigations, including selected area electron diffraction (SAED), were performed in a Cs corrected 200 kV Themis microscope (ThermoFisher) attached with an energy dispersive spectroscopy (EDS) detector. The structure of the composite was also characterized by HAADF analysis. X-ray photoelectron spectroscopic (XPS) measurements were performed using an Omicron EA 125 electron spectrometer in the "Fixed Analyzer Transmission" mode with non-monochromatized Mg Kα (1253.6 eV) radiation with resolution around 1 eV. The energy scale of the electron spectrometer was calibrated according to the ISO 15472 standard.

2.4. Electrode preparation and half-cell assembly

The composite cathodes were constructed by mixing the active materials, conductive carbon black (Super C65, Imerys), and polyvinylidene fluoride (PVDF 99.9%, Solvay), in a weight ratio of 80:10:10. The mixture was then made into a slurry with N-methyl-2-pyrrolidone (99.9%, Sigma-Aldrich) as the solvent and spread onto copper foil using an automatic film applicator (BYK Gardner GmbH). The coated electrode tape was initially dried in a hot box at 55 °C for 20 min followed by drying in a vacuum chamber at 60 °C overnight. The mass loading of sulfur on each electrode was approximate 2.6 mg/cm^2. The dried cathode tape was punched into 14 mm discs using a disc cutter (Berg & Schmid GmbH). The cathode discs were then placed in the glove box's antechamber under evacuation mode overnight before making the cells.

Coin-type cells (CR2032) were assembled inside the argon-filled glovebox with lithium-metal foil (99.9%, Sigma Aldrich) as the counter electrode as well as the reference electrode, and Whatman glass fiber as the separator. The electrolyte used was 1 M LiTFSi (99.95%, Sigma Aldrich) in 1:1 vol ratio of 1,3-dioxolane (99%, Sigma Aldrich) and 1,2-dimethoxy ethane (99.5%, Sigma Aldrich) as solvents, using no further electrolyte additives. The cells were assembled using MTI MSK 110 manual mode crimping machine.

Electrochemical impedance spectroscopy (EIS) measurements were carried out in a two-electrode cell in the frequency range from 100 kHz to 100 mHz using Bio-Logic (VSP-300) impedance analyzer at 10 mV sinus amplitude. Following EIS, the galvanostatic charge and discharge cycling of these cells was performed in a potential range of 1.5 V to 3 V (vs. Li^+/Li). All the tests were conducted at room temperature.

3. Results and discussions

3.1. Importance of freeze-drying technique in the preparation of dried GO powder

Freeze-drying, also known as lyophilization is one of the most attractive methods of "drying" for the reason that water can be used as the "porogen" to prepare uniform porous structured materials. The freeze-drying technique is the most simple and convenient way to fabricate the oriented and uniform pored structure [44]. The basic principle of lyophilization is that when the GO suspension is subjected to a very low temperature (approximately −50 °C in our case) its water content freezes to ice. This leads to an expansion of the whole volume and the particles which are initially in the close vicinity would depart from each other. The "liquid bridge" transforms into a "solid bridge" and the relative position of particles will be fixed. These particles cannot approach each other and the low interfacial tension between solid water and the particles can prevent their agglomeration in the progress of drying, i.e., sublimation of the solidified water.

Ham et al. [44] studied the freeze-drying induced changes in the structure, morphology, and chemical composition of GO and observed that the freeze-dried GO had a porous structure, maintaining the pored morphology even after high-temperature annealing. The freeze-dried samples were composed of a single folded nanosheet or a few nanosheets stacked and folded [44].

Fig S1 (a) shows the picture of GO freeze-dried at −50 °C. Before any further experiments, SEM analysis was done to confirm the porous structure of GO. The images of freeze-dried GO and the SEM are shown in the supplementary data Figs. S1(a) and S1(b) respectively. This feature is later supported by BET N_2-sorption analyses.

3.2. Physico-chemical characterization of the rGO backbones and the S/rGO composites

The specific area and the pore size distribution of rGO and RGO-S-SCC are characterized by nitrogen adsorption/desorption. The resulting isotherms are shown in Fig. 1(a–b) The isotherms are of IV types with an H_3 hysteresis loop, characteristic of slit-like pores. The calculated surface area of pristine rGO is 373.4 m^2/g and the surface area of this rGO after mixing with sulfur, with the aid of supercritical CO_2 solvent, is considerably reduced to 55.7 m^2/g. This indicates that SC-CO_2 with its gas-like diffusivity and viscosity facilitates diffusion and permeation of dissolved sulfur into the depth of micropores and mesopores very efficiently, reducing the surface area of the host rGO to a considerable extent. In this preliminary analysis, we can see the beneficial role of the supercritical CO_2 medium in enabling efficient intercalation of the active sulfur particles into the porous rGO.

Fig. 2 shows the morphology and structure of the rGO/sulfur composite cathode analyzed under HR-SEM. Fig. 2(a–c) indicates the lamellar structure of pristine reduced graphene oxide and the microstructural changes induced by the infusion of sulfur into this rGO with the aid of SC-CO_2 is evident in Fig. 2(d–f). It can be seen that fragmentation of composite particles has occurred upon SC-CO_2 assisted infusion process resulting in platelet-like morphology. The homogenous spatial distribution of carbon and sulfur in the composite can be seen from the elemental maps as shown in Fig. 2(g–h).

To study the internal microstructure and composition of the as-prepared rGO/sulfur composites with enhanced resolution and to determine the interplanar distances of rGO before and after the SC-CO_2 treatment, high-resolution TEM (HR-TEM), energy dispersive spectroscopy and selected area electron diffraction (SAED) analysis were performed and the results are shown in Fig. 3(a–f). The sample preparation for TEM was done by focussed ion beam technique (FIB). The recorded EDS spectrum (not shown) of RGO-S-SCC clearly shows the presence of major elements carbon and sulfur. The interplanar distance (d) for the samples is determined by SAED analysis. The d value for basal planes is 0.388 nm both in the pristine rGO and in the sulfur encapsulated RGO-S-SCC. The result indicates that sulfur incorporates in form of nanoparticles (as illustrated in the graphical abstract) rather than intercalated atoms between the sheets, leaving the structure of the GO intact. In the high-resolution HAADF-STEM image (Fig. S4) the brighter contrast is produced by the heavier elements (In this case sulfur compared to carbon). The images reveal the presence of atomic or cluster of sulfur nanoparticles in the pores of rGO. This shows how the rGO can serve as a good host to encapsulate sulfur and sulfur-lithium clusters during charge-discharge reactions [85].

The sulfur content of the RGO-S-SCC and RGO-S-SCC 250 composites is determined through TG-DSC analysis. As shown in Fig. 4(a), the composite shows a sulfur loading of 67.61%.

According to the analysis, there are mainly three mass loss steps on the TG curve, the first one, with roughly half a percent of mass loss, could be the evaporation of a small amount of physically bound water. The next, largest mass loss between 125 °C and 440.6 °C accompanied by a small and broad endotherm is due to the evaporation of the sulfur content from the rGO/S composite, while the last mass loss is the result of the slow thermal oxidation of the remaining carbon.

The phase structures of rGO, pure S powder, and RGO-S-SCC samples are analyzed by XRD. As 'can be seen in Fig. 4(b), the original, pure sulfur powder shows sharp diffraction peaks corresponding to the crystalline S_8 structure and the pristine rGO shows broad diffraction peaks corresponding to its amorphous nature. But it can be observed that for the composite of rGO and sulfur, after the SC-CO_2 treatment no diffraction peaks corresponding to sulfur are visible, resulting in a similar pattern to that of pristine rGO. This is because, during the SC-CO_2 encapsulation of sulfur inside the pores or rGO, the highly crystalline sulfur becomes amorphous leaving no diffraction peaks [45]. These results are further substantiated by Raman spectroscopic analysis. According to Fig. 4(c), the pristine sulfur shows a series of Raman peaks owing to the vibration of S–S bonds in the crystalline S_8 class [45]. The spectra for both rGO, and RGO-S-SCC are similar. Essentially no peaks corresponding to sulfur are observed for RGO-S-SCC which is an indication that the sulfur is no longer possessing crystalline nature since it has transformed into an amorphous state. These results are good indicators to demonstrate how the synthesis of carbon/sulfur composite with the assistance of SC-CO_2 helps in the effective trapping and homogenous distribution of sulfur nano particles inside the carbon matrix.

XPS analysis was done in order to identify the surface composition and chemical states of the RGO-S-SCC composite and the rGO used in this work in comparison with conventional carbon black (which might be commonly used in Li–S battery cathodes). The results are summarized in Table 1, the C 1s spectra of the samples are presented in Fig. 5A while the S 2p spectrum of the RGO-S-SCC composite is shown in Fig. 5B.

Looking at the data reported in Table 1, the carbon black sample consists of essentially pure carbon with minimal traces of oxygen moieties. The corresponding C 1s spectrum (Fig. 5A, curve (a) possesses the slightly asymmetric peak shape characteristic of graphitic carbon with its maximum around 284.4 eV binding energy, in good agreement with literature data [48]. The tiny O 1s peak is located at 532.7 eV binding energy, which suggests the presence of OH-like functional groups on the carbon backbone [46]. As expected, the rGO used in this study contains a relatively

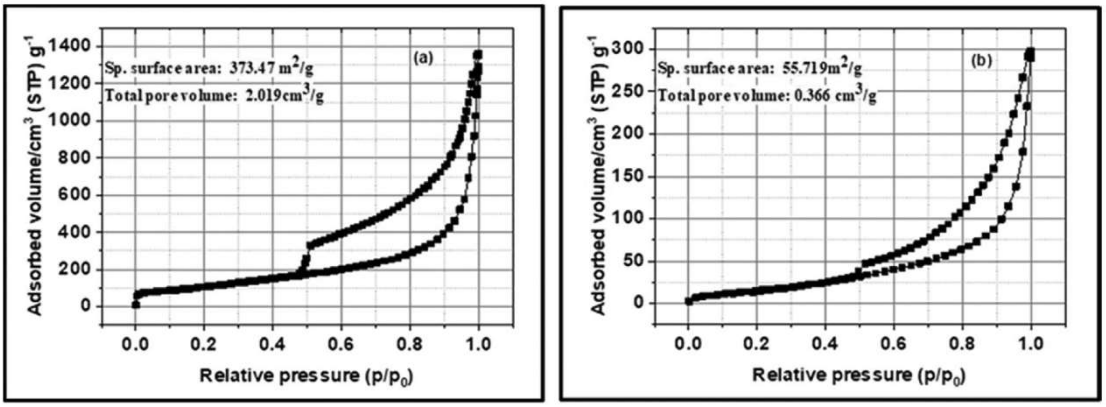

Fig. 1. N_2 adsorption-desorption isotherm curves for (a) rGO and (b) RGO-S-SCC.

high amount of functional groups, which enhances the asymmetry of the C 1s envelope towards high binding energies (Fig. 5A, curve (b)). In addition to the graphitic carbon line shape, two smaller contributions can be identified. The stronger one at 286.0 eV is due to carbon singly-bound to oxygen like in C—OH groups or C—*O*—C-like arrangements such as in epoxide groups or lactones. The weaker high binding energy component at 288.3 eV can be assigned to more highly oxidized carbon species such as carboxylic or anhydride functionalities or carbon atoms bound to more than one oxygen atom in lactones [46,47]. The amount of C atoms singly-bound to O is around 13% of the total C content while the strongly oxidized C atoms account for 5%, indicating the high functional group content of the material. The O 1s spectrum of the rGO sample is in tentative agreement with the C 1s spectrum, indicating presence of oxygen species in a range of different bonding environments. The tiny Na and Mn content probably arises from the remnants of chemicals used for GO synthesis. According to Table 1 and Fig. 5A (curve (c)), sulfur loading resulted in relatively minor changes in the carbonaceous part of the composite: only a minor loss of the oxygen-containing functionalities can be observed.

Information on the chemical structure of the encapsulated sulfur within the rGO is shown in Table 1 and Fig. 5B. The main contribution of the S 2p spectrum arises from a $2p_{3/2}$-$2p_{1/2}$ spin-orbit doublet with its leading peak at 163.5 eV, which is characteristic for elemental sulfur [48], confirming the predominance of S—S bonds in the composite. The other well-defined S 2p peak is significantly broader and is located at 167.8 eV binding energy corresponding to oxidized sulfur, although literature data overlap in this binding energy range for many oxidized sulfur forms, involving sulfonyl (SO_2), sulfonate (SO_3) or sulfate (SO_4) functionalities [48].

In summary, the characterization of the RGO-S-SCC composite confirmed the successful sulfur loading of rGO by the supercritical CO_2 treatment. Thermogravimetry confirmed that the desired amount of sulfur was driven into the rGO. SEM/EDS studies indicated a relatively homogeneous large scale sulfur distribution along with a few large agglomerates, while XPS data suggested formation of larger sulfur particles and/or encapsulation by carbon. XRD as well as Raman spectroscopy revealed the formation of amorphous sulfur deposits while XPS indicated the predominance of elemental sulfur in the system along with a low amount of oxidized species.

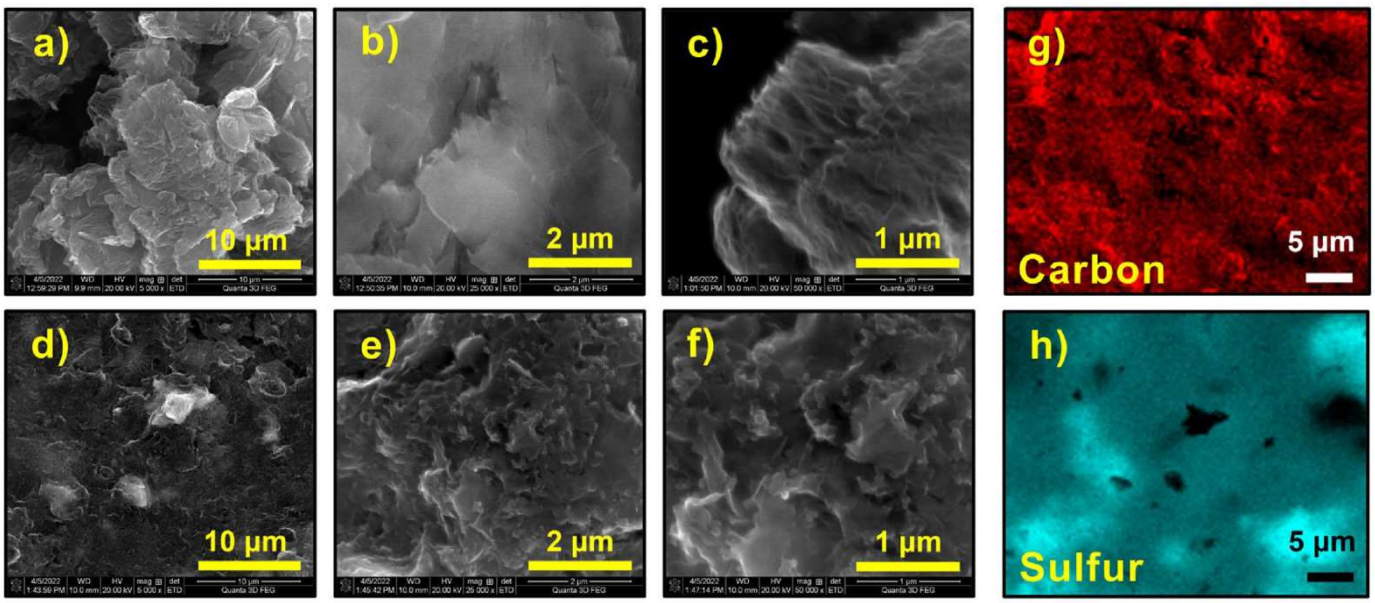

Fig. 2. SEM images of (a—c) rGO (d—f) RGO-S-SCC in different magnifications, and (g—h) Elemental maps of carbon and sulfur in RGO-S-SCC.

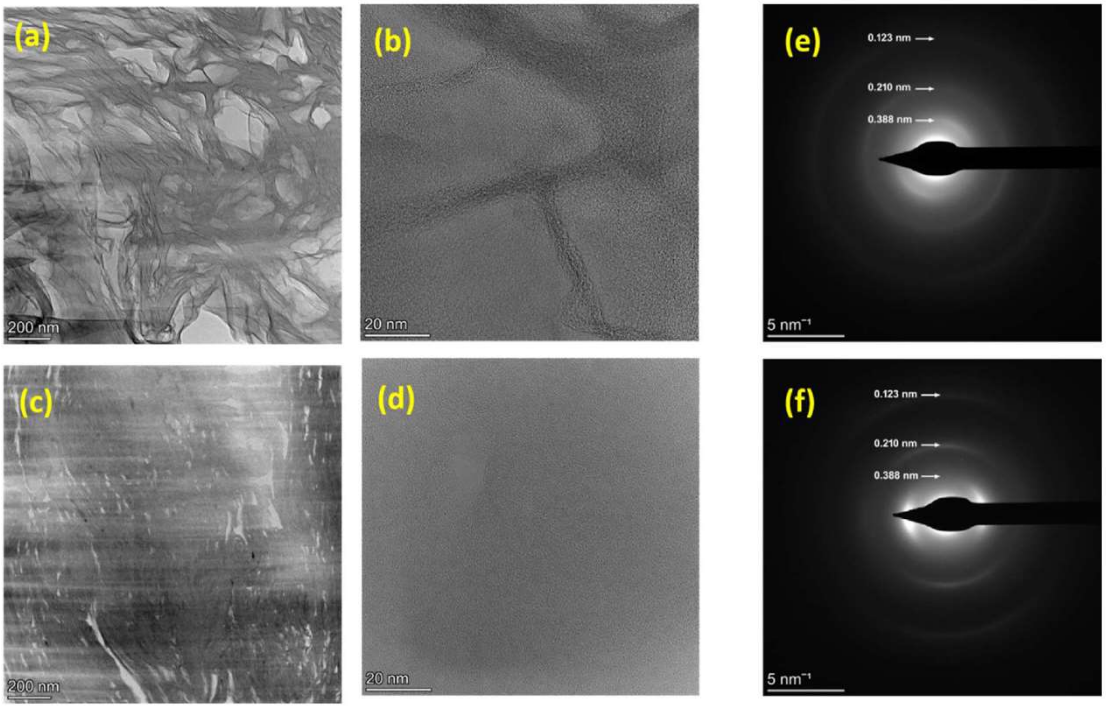

Fig. 3. HR-TEM images of (a–b) rGO, (c–d) RGO-S-SCC in different magnifications, (e–f) SAED patterns of rGO and RGO-S-SCC respectively.

3.3. Electrochemical performance evaluation of the prepared half-cells

Fig. 6 shows the comparative electrochemical impedance spectra (complex-plane impedance plots) of the as-prepared CR 2032-coin cell with Li metal anode, 1 M Lithium bis (trifluoromethanesulfonyl) imide (LiTFSi) in 1,2-dimethoxyethane (DME) and 1,3-dioxalane (DOL) (1:1 vol ratio) electrolyte and cathodes prepared by the conventional melt-diffusion technique (S/C Composite) and SC-CO_2 treatment (RGO-S-SCC and RGO-S-SCC 250). The electrochemical impedance measurements have been carried out in the frequency range of 100 kHz-100 mHz, with 10 mV sinusoid voltage perturbation at open circuit potential. The impedance spectra are validated using the linearized Kramers-Kronig (K–K) test [52] to verify that the linearity, causality, stability, and finiteness of the data are maintained. Only data with relative residuals below 1.5% are used for further calculations. Because the impedance spectra of batteries can sometimes be very complex, distribution of relaxation times (DRT) analysis method is a possible approach to interpret complex EIS data.

Additionally, EIS is often evaluated by complex nonlinear least-squares (CNLS) fitting method, which is computed by a system model called an electrical equivalent circuit, where each parameter of the circuit is identical with a physical characteristic of the system under investigation. However, the choice of an electrical circuit requires prior knowledge of the impedance of each element. DRT analysis is used to transform the impedance data from the frequency domain (f) to the time domain (t), thus obtaining the distribution function of the time constants involved in the system from the frequency-dependent impedance data. DRT can be considered as a tool to help finding a suitable model and its initial parameters that should be used to fit impedance data. To calculate the DRT spectrum by inverting the data, it is required to solve the Fredholm integral equation, which is an ill-posed problem. Different approaches exist to obtain solution to an ill-posed problem such as Fourier transformation [49], Bayesian approach [50–52], Ridge and Lasso [53] methods etc. But one of the best techniques is the Tikhonov regularization [54–56]. In present study the Tikhonov regularization method was used on the Kramers-Kronig transformable region of the spectrum with $\lambda = 0.001$

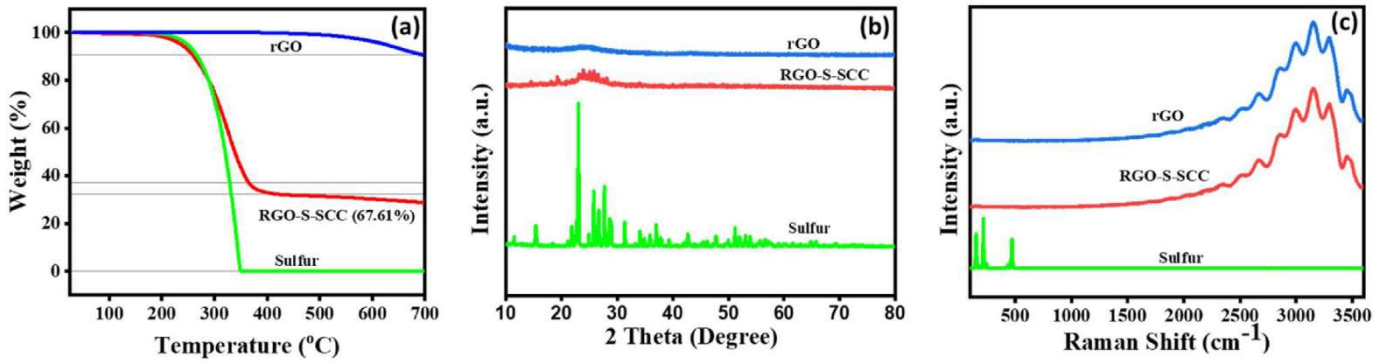

Fig. 4. (a) TG curves, (b) XRD patterns and (c) Raman spectra of pure sulfur, pure rGO, and RGO-S-SCC.

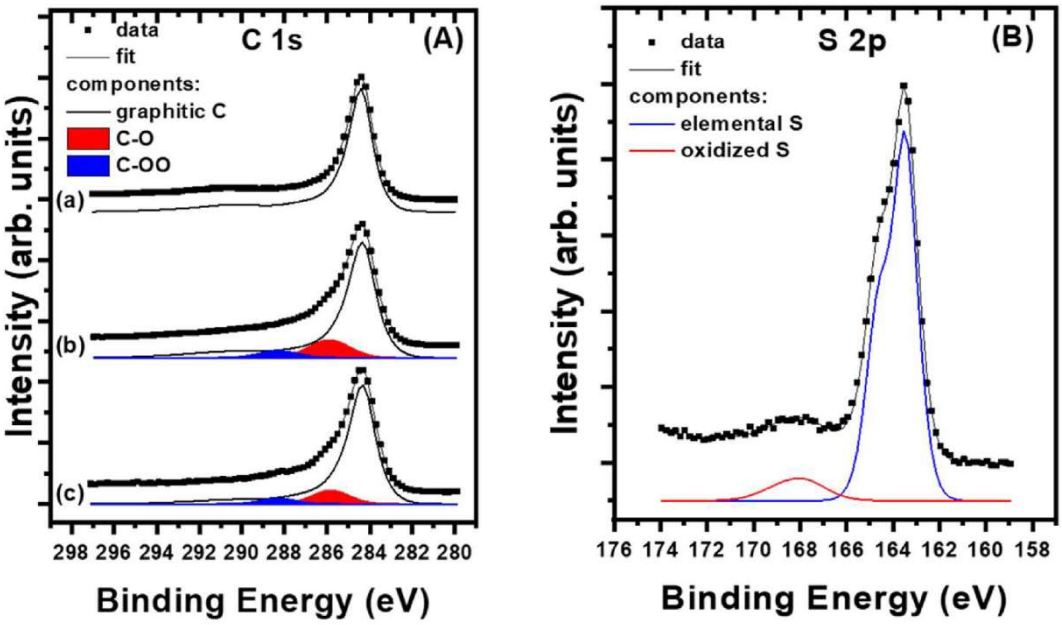

Fig. 5. (A): C1s XPS spectra of (a): Carbon Black, (b): rGO, (c): RGO-S-SCC. (B): S 2p spectrum of RGO-S-SCC.

regularization parameter in all case and the obtained DRT spectra are shown in Fig. 7.

It can be seen from the DRT spectra that all the system concerned in present work contains at least four different time constants (τ). The time constants are associated with different charge transfer processes (in the high - and middle-frequency region) or diffusion impedance (at low frequency region). The applied model describes the system with a series resistance (R_S) which describes the electrolyte resistance which can be observed in the high-frequency part of the impedance spectra. According to the DRT analysis the system contains the interface resistance $P1$ between lithium metal anode and electrolyte, the charge transfer $P2$ between cathode and electrolyte, the contact resistance $P3$ between cathode and current collector and the solid-state diffusion $P_{diff,Q}$ in the cathode active material. The diffusion element in this model is the so-called de Levie ($Z_{deLevie}$) element or transmission line element. The reason for the application of this element in the modeling process is that the surface of the applied materials is not completely flat rather a rough surface.

$$Z_{de\ Levie} = \sqrt{R_{ion}Z_S}\coth\sqrt{\frac{R_{ion}}{Z_S}}$$

The element Z_S can be expressed as $Z_s = Q_S(1j \bullet \omega)^{\gamma}$ where Q_s is a constant phase element and γ is the exponent of the constant phase element Q_s based on ref [57].

The total impedance equations contain:

$$Z_{tot} = R_S + Z_{RQ1} + Z_{RQ2} + Z_{RQ3} + Z_{deLevie}$$

The complex nonlinear least-squares fitting of the model with Levenberg-Marquard algorithm was carried out in a self-written code in Python 3 with standard scientific packages (NumPy, SciPy, Pandas, Lmfit and Matplotlib). The results are shown in Fig. 8(a) with the schematic diagram of the fitted model.

The χ^2 value of the fitting was below 10^{-8} in all case. Table 2 contains the results from the CNLS fitting of the impedance spectra. As clear from Table 2, the obtained resistances of the rGO/S composites are significantly smaller (with 1 and 2 orders of magnitude) in comparison with the S/C composite prepared by melt diffusion technique using the carbon black matrix. Furthermore, in previously reported work on the supercritical CO_2 assisted synthesis [38,45], the activated S/C composite cathodes showed resistances ranging from 270 Ohm to 1330 Ohm, which are much higher values of resistances compared to the ones obtained in this

Table 1
XPS data on surface composition and chemical states of carbon black, reduced graphene oxide and sulfur-reduced graphene oxide composite.

	Carbon Black			rGO			RGO-S-SCC		
	BE	assignment	amount (at%)	BE	Assignment relative contributions	amount (at%)	BE	Assignment, relative contributions	amount (at%)
C 1s	284.4	graphitic C	99.5	284.4 286.0 288.3	graphitic C (82%) C–OH/C–O–C (13%) carboxyls (5%)	85.6	284.4 285.8 288.3	graphitic C (86%) C–OH/C–O–C (10%) carboxyls (4%)	76.4
O 1s	532.7	C–OH	0.5	531.0 533.3 535.9	C–O–C (41%) carboxylic, lactone or ether groups (48%) moisture (11%)	13.0	531.1 533.2 536.0	C–O–C, S–O (46%) carboxylic, lactone or ether groups (47%), moisture (7%)	14.0
S $2p_{3/2}$	–	–	–	164.0 168.8	elemental S SO_3, SO_4	0.4	163.5 167.8	elemental S (92%) SO_2, SO_3, SO_4 (8%)	8.8
Na 1s	–	–	–	1071.8	ionic Na	0.6	1071.6	ionic Na	0.8
Mn $2p_{3/2}$	–	–	–	641.7	Mn^{2+}:MnO, $Mn(OH)_2$	0.4	–	–	–

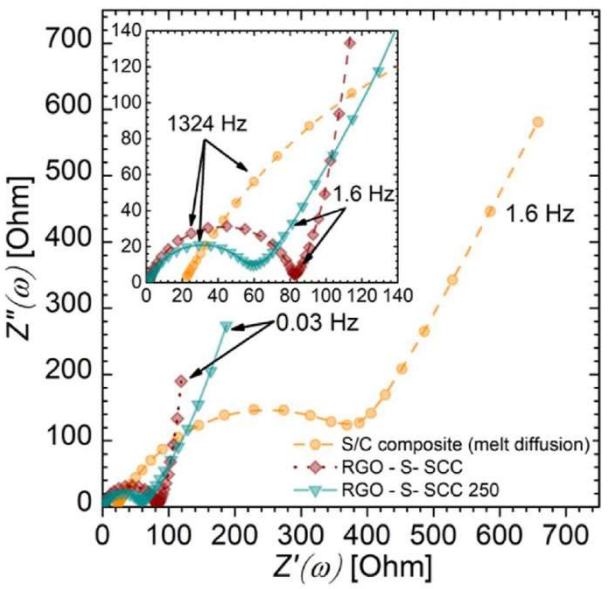

Fig. 6. Complex-plane impedance plots of the S/C composite, rGO/S nonheated (RGO-S-SCC) and rGO/S heated (RGO-S-SCC 250) composite samples in the frequency range of 100 kHz-100 mHz.

work. The higher resistance values of activated S/C composites can be due to the weaker interaction of the sulfur with the carbon matrix. In contrast to this, for the as prepared composite cathodes, RGO-S-SCC and RGO-S-SCC 250, significantly lower impedances can be explained as follows. Since SC-CO_2 has low interfacial tension and high diffusivity, the surface tension interface between carbon matrices and SC-CO_2 is very low. This enables better wetting of pores of rGO, resulting in more near contact of the highly dispersed/dissolved sulfur particles impregnated within rGO.

The charge-discharge profiles of the as-prepared cells are shown in Fig. 9(a) and (b) where all the charge and discharge curves display well-defined voltage plateaus. The cells with RGO-S-SCC and RGO-S-SCC 250 cathodes were cycled in a potential range of 1.5 V−3 V. To have much more comprehensible information on how the cells perform under extreme conditions, they are subjected to 200 charge-discharge cycles and at different current densities. At 0.1C rate, the fabricated RGO-S-SCC cell shows an initial discharge capacity of 1024 mAh/g. The cell shows very good capacity retention of 92.28% delivering a discharge capacity of 945 mAh/g after 200 charge-discharge cycles. The developed RGO-S-SCC cells showed excellent performance with a fairly low decay of 0.04% per cycle even after 200 charge-discharge cycles.

The RGO-S-SCC 250 sample was studied only to understand whether there is any significant influence for the heat treatment of the composite on the electrochemical performance. But it was observed that, there wasn't any significant differences, but showed almost similar electrochemical behaviour to RGO-S-SCC. RGO-S-SCC 250 cell shows an initial discharge capacity of 978 mAh/g cycling at 0.1C rate. The discharge capacity after 200 charge-discharge cycles is 909 mAh/g corresponding to a capacity retention of 92.94%.

The cycling stability and the coulombic efficiency of the RGO-S-SCC and RGO-S-SCC 250 cells at 0.1C rate for 200 cycles are shown in Fig. 9(c−d). Coulombic efficiency which is the ratio of the discharge capacity over the charge capacity of the cells is maintained at approximately 99.5% even after prolonged cycling. This high Coulombic efficiency is a scalar indicator for the good electrochemical reversibility of the battery electrode function. The rate performance of the cell subjected to lower and higher current rates is shown in Fig. 9(e).

Table 3 compares data on the rate performances of the cells reported previously based on SC-CO_2 assisted synthesis of S/C composite, with the current work. It can be clearly seen that the stability and rate performance is outstanding in the case of cells from RGO-S-SCC electrode. In our case, the discharge capacity of the cells is enhanced by approximately 52−59% at 1C rate and 69−80% at 2C rate in comparison with the other works. The cells could maintain cycling stability with very little capacity degradation even after 200 charge-discharge cycles.

Fig. 9(f) shows a comparison plot on the long-term charge-discharge cycling profile (at 0.1C rate) of the S/C composite cathode prepared by the conventional melt diffusion with carbon black (denoted as S/C Melt Diff in the figure) with that of the RGO-S-SCC composite cathode with rGO as the sulfur host. From the figure, it is clear that the polarization effects in S/C Melt diff are much higher than the RGO-S-SCC, which is in agreement with the impedance spectrum analysis (Fig. 6), where S/C Melt diff showed much higher resistance. Most importantly, the reversible capacity of the RGO-S-SCC cells is significantly higher in comparison with S/C Melt Diff. Such boosted electrochemical performance of the investigated cells with respect to the reversible capacity, long-term cycling stability, and high coulombic efficiency can be explained as follows. As mentioned previously, XPS analysis of rGO revealed the strong presence of polar functional groups (epoxy, carboxylic groups, etc.).

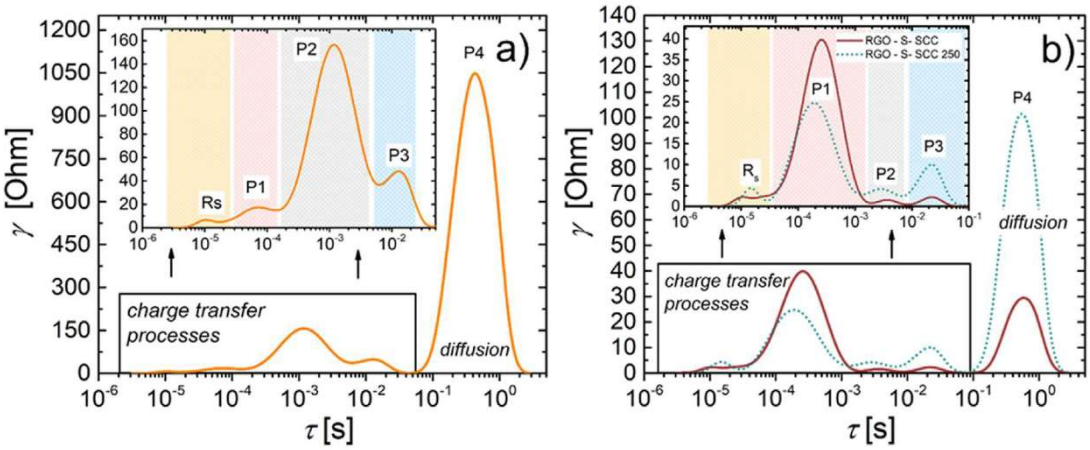

Fig. 7. DRT spectra obtained with λ = 0.001 regularization parameter in the case of a) S/C composite (melt diffusion), b) RGO-S-SCC and RGO-S-SCC 250 electrodes.

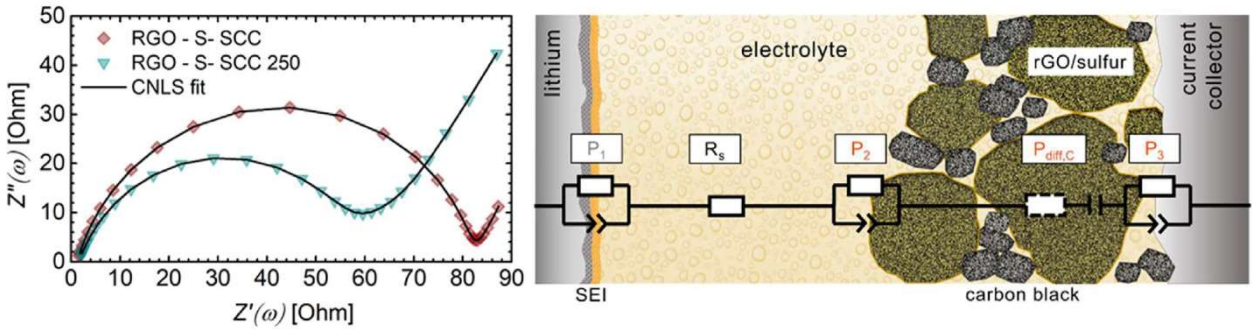

Fig. 8. Complex-plane impedance spectra of the RGO-S-SCC and RGO-S-SCC 250 with the CNLS fitting results and the illustration of all identified mechanisms and corresponding physical interpretation in half-cells including: The electrolyte resistance (R_s), the interface resistance P_1 between lithium metal anode and electrolyte, the charge transfer P_2 between cathode and electrolyte, the contact resistance P_3 between cathode and current collector, and the solid state diffusion $P_{diff,Q}$ in the cathode active material.

The presence of these oxygen-containing functional groups in rGO acts as sulfur immobilizers that can anchor sulfur atoms within the conducting carbon matrix [58–60]. So, even during prolonged charging and discharging, due to this strong interaction of rGO and sulfur, the lithium polysulfide discharge products will be confined within the cathode itself without getting dissociated in the electrolyte and diffusing towards the Li metal anode. This helps curtail the polysulfide shuttling back and forth between the electrodes. This in turn benefits from maximum active material utilization and the least active material loss, resulting in highly reversible and stable cells with ultra-low-capacity degradation over prolonged cycling.

This phenomenon is evident from the difference in the charge-discharge voltage profiles of S/C Melt Diff and RGO-S-SCC (cf. Fig. 9(f)). Related to the S/C Melt diff sample, the voltage plateau corresponding to the formation of the higher-order lithium polysulfides (marked 1 and 2 related to the discharge and charge curves, respectively) is visible, however, this is missing for the RGO-S-SCC electrode in the voltage profile. The nature of the charge discharge plots largely depends on the microstructure (porosity, heteroatom content etc.) of the carbon host and the adsorption capability of the carbon host for the sulfur and Li - polysulfides formed during the charge-discharge reaction. The influence of microstructure of carbon and its adsorption capability on the electrochemical performance is reported previously [84]. Here, the obtained discharge plateau of RGO-S-SCC is the distinctive characteristic of the microporous reduced graphene oxide matrix to which the sulfur is embedded. The rGO, with the presence of polar functional groups serves as strong adsorbing host to the Li-polysulfides and restricts/eliminates the discharge potential hysteresis (which is indicated by higher voltage plateau) formed during the electrochemical reaction. Hence, only lower voltage plateau is observed.

Since higher-order, i.e., long-chain lithium polysulfides are quite soluble in the organic electrolyte their presence can be detrimental to the long-term cycling performance of the Li–S batteries due to diffusion phenomena. The fast degradation and breakdown of the higher-order lithium polysulfides into lower-order (short-chain) polysulfides may result in more stable cycling behaviour by suppressing polysulfide migration. The rGO host in our case besides its molecular anchoring by its polar domains can provide a catalytic effect to rapidly decompose long-chain polysulfides. It is obvious from the voltage profile data presented in Fig. 9(f)., that rGO-based sulfur-containing nanocomposite cathode provides an alternative mechanism for the sulfur→ polysulfide → lithium sulfide transformation [61–63].

In addition to this chemical confinement effect, the SC-CO_2 treatment enables the physical confinement of sulfur into the depths of the micropores of the rGO. Thereby, simultaneous chemical and physical confinement of the polysulfide species can occur in our rGO based nanocomposite cathode during the electrochemical cycling. The above results demonstrate the synergistic effects of utilizing *i)* supercritical CO_2 technology and *ii)* rGO carbon host by the design of C/S nanocomposites for Li–S rechargeable batteries. This allows the design and synthesis of Li–S cathode which is capable of physical confinement of the Li-polysulfides by creating porous electrodes with high tortuosity and porosity and also the chemical confinement of Li-polysulfides is feasible due to the polar functional groups on the carbonaceous sulfur host. This, in turn, helps to prepare highly efficient carbon/sulfur nanocomposite cathode materials for Li–S batteries with outstanding performance.

Table 2
CNLS fitting of the impedance spectra.

CNLS fitting results with standard errors of the estimated parameters			
Parameter	S/C composite (Melt diffusion)	RGO-S-SCC 250	RGO-S-SCC
R_s [Ohm]	19.77 ± 0.46	1.27 ± 0.44	1.21 ± 0.40
R_1 [Ohm]	182.41 ± 4.98	56.06 ± 0.77	60.61 ± 0.35
Q_1 [F]	$3.21\bullet10^{-5} \pm 4.2\bullet10^{-6}$	$1.87\bullet10^{-5} \pm 0.3\bullet10^{-6}$	$1.08\bullet10^{-5} \pm 1.1\bullet10^{-6}$
n_1	0.72	0.8	0.9
R_2 [Ohm]	152.61 ± 5.51	0.22 ± 0.06	9.35 ± 0.27
Q_2 [F]	$2.79\bullet10^{-5} \pm 3.6\bullet10^{-6}$	$4.01\bullet10^{-6} \pm 3.2\bullet10^{-7}$	$5.84\bullet10^{-5} \pm 9.2\bullet10^{-6}$
n_2	0.9	0.9	0.9
R_3 [Ohm]	500 ± 3.71	4.42 ± 0.41	9.30 ± 0.06
Q_3 [F]	$1.42\bullet10^{-3} \pm 3.5\bullet10^{-4}$	$3.50\bullet10^{-3} \pm 2.6\bullet10^{-4}$	$5.56\bullet10^{-5} \pm 3.2\bullet10^{-6}$
n_3	0.7	0.9	0.8
R_{ion} [Ohm]	83.31 ± 8.25	1.37 ± 0.40	4.97 ± 0.58
Q_s [F]	$4.51\bullet10^{-4} \pm 2.5\bullet10^{-5}$	$5.68\bullet10^{-3} \pm 0.1\bullet10^{-4}$	$2.03\bullet10^{-2} \pm 0.6\bullet10^{-6}$
γ	0.8	0.7	0.7

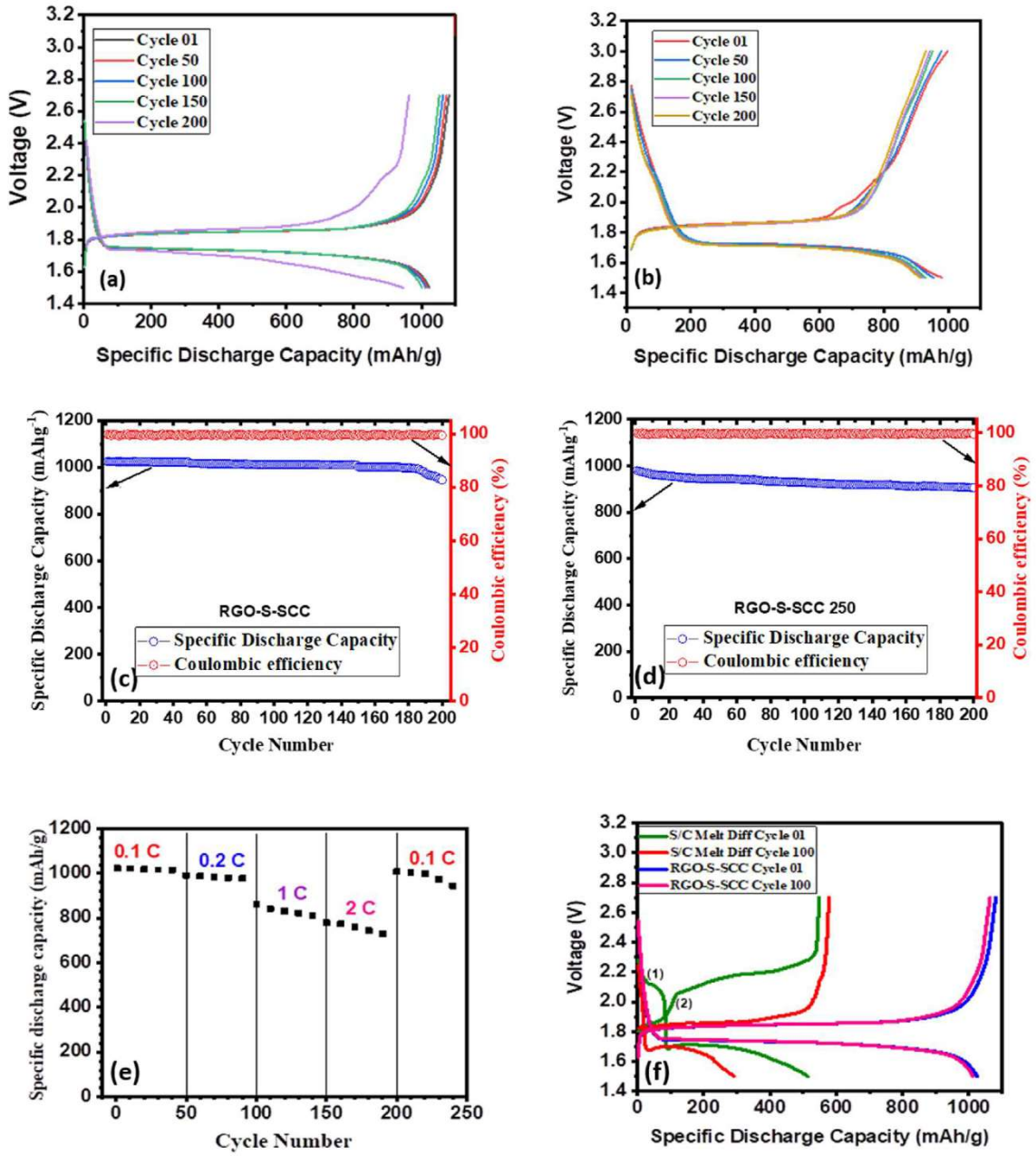

Fig. 9. (a) Charge -discharge voltage profiles of RGO-S-SCC @ 0.1C rate; (b) Charge -discharge voltage profiles of RGO-S-SCC 250 @ 0.1C rate; (c) Long term cycling performance of RGO-S-SCC @ 0.1C; (d) Long term cycling performance of RGO-S-SCC 250 @ 0.1C rate; (e) rate performance plot of the RGO-S-SCC electrode; (f) Comparison plot of voltage profiles for composite cathodes prepared by S/C melt Diff and RGO-S-SCC.

4. Conclusion

In this study, a facile, low cost, environmentally benign and room temperature SC-CO_2 synthesis technique has been exploited to fabricate a high-performance C/S composite cathode for Li–S batteries. Herein, we utilized the prominent properties of reduced graphene oxide (rGO) as the sulfur host to fabricate rGO/sulfur composite (RGO-S-SCC and RGO-S-SCC 250) cathode for Li–S batteries. Taking into account the remarkable features such as hydrophobicity, high infiltrability, diffusivity, and solvability, SC–CO_2–assisted synthesis helped in achieving efficient and homogenous physical confinement of sulfur in rGO matrix. Due to the

Table 3
Comparative study on the rate performance of RGO-S-SCC electrode with previously reported works on supercritical CO_2 assisted synthesis of S/C.

	Specific Discharge Capacity at different Current Rates					Capacity degradation (%)/Number of cycles
	0.1C	0.2C	1C	2C	0.1C	
ref [45]	844	733	446	156	676	19/150
ref [38]	882	697	381	242	762	13/100
Present study*	***1024***	***991***	***929***	***780***	***945***	***9/200***

sudden pressure release process, the SC-CO_2 expands the interlayers of rGO creating much additional space for dissolved sulfur to be encapsulated ensuring strong interaction between the sulfur and carbon matrices. Concurrently, the presence of functional groups in the rGO enables the immobilization of sulfur, resulting in the chemical confinement of soluble lithium polysulfides within the cathode. Owing to these integrated characteristics, the developed cells with RGO-S-SCC cathode, Li metal anode, and 1 M LiTFSi in DME and DOL (1:1 vol ratio) electrolyte showed outstanding electrochemical performance with respect to specific capacity, Coulombic efficiency, and stable cycle life even at higher current rates for prolonged cycling. The cell showed excellent capacity retention of 92.2% delivering an initial discharge capacity of 1024 mAh/g and a discharge capacity of 945 mAh/g after 200 charge-discharge cycles at 0.1C rate. The developed cells showed high-rate performance with an ultralow decay of 0.03% per cycle even after 200 charge-discharge cycles. Moreover, the highly sustained Coulombic efficiency (around 99.5%) is a scalar indicator of the good electrochemical reversibility of the battery electrode function. It can be deduced from the results that this less investigated, facile and sustainable approach of SC-CO_2 assisted synthesis provides new insight into the rational design and controllable synthesis of carbon/sulfur composite cathodes for Li–S batteries. More optimization and fine tuning of the experimental conditions (pressure, treatment time etc.) of SC-CO_2 infusion and the structural modifications of rGO has to be done in order to have an in-depth understanding for further development of Li–S cathode systems with enhanced electrochemical performance.

Credit authorship distribution statement

Shiva Shankar Lakshmi: Methodology, Validation, Investigation, Analysis, Writing-original draft; **Dóra Zalka**: Investigation, Software development, Modeling, and its analyses; **Tamás Szabó**: Resources, Investigation**; Katalin Balázsi, Levente Illés, Zsolt Czigány and Zoltán Pászti**: Investigation; **Edit Székely**: Resources; **Márton Kőrösi**: Resources, Validation; **Robert Kun**: Conceptualization, Funding acquisition, Review and Editing, Supervision.

Declaration of competing interest

The authors declare that they have no known competing financial interests or personal relationships that could have appeared to influence the work reported in this paper.

Data availability

Data will be made available on request.

Acknowledgments

The authors thank the financial support from Project no. RRF-2.3.1-21-2022-00009, titled National Laboratory for Renewable Energy that has been implemented with the support provided by the Recovery and Resilience Facility of the European Union within the framework of Programme Széchenyi Plan Plus.

The authors also thank the financial support from Project No. 124851, that has been implemented with the support provided from the National Research, Development and Innovation Fund of Hungary (NKFIH), financed under FK funding scheme.

The Authors thank the instrumentation facility of Research Center for Natural Sciences (TTK) with the kind support of Laszló Trif for TG-DTA analysis, Ágnes Szegedi for BET analysis, Eszter Bódis for XRD analysis and Judit Mihály for Raman analysis. The authors thank Zoltán Dankházi, Eötvös Loránd University Budapest for SEM-EDX instrumentation support.

The authors thank Hala Roumia, University of Szeged and János Béri, Faculty of Chemical Technology and Biotechnology, Budapest University of Technology and Economics for experimental support. This research was supported by the grant no. VEKOP-2.3.3-15-2016-00002 and VEKOP-2.3.2-16-2016-00011 of the European Structural and Investment Funds.

Appendix A. Supplementary data

Supplementary data to this article can be found online at https://doi.org/10.1016/j.mtchem.2022.101240.

References

[1] A. Manthiram, Y. Fu, Y. Su, Challenges and prospects of lithium-sulfur batteries, Acc. Chem. Res. 46 (2013) 1125–1134.
[2] L. Ji, M. Rao, H. Zheng, L. Zhang, Y. Li, W. Duan, J. Guo, E.J. Cairns, Y. Zhang, Graphene oxide as a sulfur immobilizer in high performance lithium/sulfur cells, J. Am. Chem. Soc. 133 (2011) 18522–18525, https://doi.org/10.1021/ja206955k.
[3] X. Ji, K.T. Lee, L.F. Nazar, A highly ordered nanostructured carbon-sulphur cathode for lithium-sulphur batteries, Nat. Mater. 8 (2009) 500–506, https://doi.org/10.1038/nmat2460.
[4] C. Lai, X.P. Gao, B. Zhang, T.Y. Yan, Z. Zhou, Synthesis and electrochemical performance of sulfur/highly porous carbon composites, J. Phys. Chem. C 113 (2009) 4712–4716, https://doi.org/10.1021/jp809473e.
[5] H.S. Ryu, H.J. Ahn, K.W. Kim, J.H. Ahn, J.Y. Lee, Discharge process of Li/PVDF/S cells at room temperature, J. Power Sources 153 (2006) 360–364, https://doi.org/10.1016/j.jpowsour.2005.05.037.
[6] J.L. Wang, J.Y. Yang, J.Y. Xie, N.X. Xu, Y. Li, Sulfur–carbon nano-composite as cathode for rechargeable lithium battery based on gel electrolyte, Electrochem. Commun. 4 (2002) 499–502, https://doi.org/10.1016/S1388-2481(02)00358-2.
[7] X. Ji, S. Evers, R. Black, L.F. Nazar, Stabilizing lithium-sulphur cathodes using polysulphide reservoirs, Nat. Commun. 2 (2011), https://doi.org/10.1038/ncomms1293.
[8] H. Wang, Y. Yang, Y. Liang, J.T. Robinson, Y. Li, A. Jackson, Y. Cui, H. Dai, Graphene-wrapped sulfur particles as a rechargeable lithium-sulfur battery cathode material with high capacity and cycling stability, Nano Lett. 11 (2011) 2644–2647, https://doi.org/10.1021/nl200658a.
[9] G. He, X. Ji, L. Nazar, High "c" rate Li-S cathodes: sulfur imbibed bimodal porous carbons, Energy Environ. Sci. 4 (2011) 2878–2883, https://doi.org/10.1039/c1ee01219c.
[10] J. Hassoun, B. Scrosati, A high-performance polymer tin sulfur lithium ion battery, Angew. Chem. 122 (2010) 2421–2424, https://doi.org/10.1002/ange.200907324.
[11] V.S. Kolosnitsyn, E.V. Karaseva, Lithium-sulfur batteries: problems and solutions, Russ. J. Electrochem. 44 (2008) 506–509, https://doi.org/10.1134/S1023193508050029.
[12] Y. Yang, M.T. McDowell, A. Jackson, J.J. Cha, S.S. Hong, Y. Cui, New nano-structured Li_2S/Silicon rechargeable battery with high specific energy, Nano Lett. 10 (2010) 1486–1491, https://doi.org/10.1021/nl100504q.
[13] J. Shim, K.A. Striebel, E.J. Cairns, The lithium/sulfur rechargeable cell, J. Electrochem. Soc. 149 (2002) A1321, https://doi.org/10.1149/1.1503076.
[14] Y.J. Choi, Y.D. Chung, C.Y. Baek, K.W. Kim, H.J. Ahn, J.H. Ahn, Effects of carbon coating on the electrochemical properties of sulfur cathode for lithium/sulfur cell, J. Power Sources 184 (2008) 548–552, https://doi.org/10.1016/j.jpowsour.2008.02.053.
[15] C. Liang, N.J. Dudney, J.Y. Howe, Hierarchically structured sulfur/carbon nanocomposite material for high-energy lithium battery, Chem. Mater. 21 (2009) 4724–4730, https://doi.org/10.1021/cm902050j.
[16] X. Ji, L.F. Nazar, Advances in Li-S batteries, J. Mater. Chem. 20 (2010) 9821–9826, https://doi.org/10.1039/b925751a.
[17] X.P. Gao, H.X. Yang, Multi-electron reaction materials for high energy density batteries, Energy Environ. Sci. 3 (2010) 174–189, https://doi.org/10.1039/b916098a.
[18] X.Q. Zhang, C. Liu, Y. Gao, J.M. Zhang, Y.Q. Wang, Research progress of sulfur/carbon composite cathode materials and the corresponding safe electrolytes for advanced Li-S batteries, Nano 15 (2020) 1–13, https://doi.org/10.1142/S1793292020300029.
[19] L. Zhang, Y. Wang, Z. Niu, J. Chen, Advanced nanostructured carbon-based materials for rechargeable lithium-sulfur batteries, Carbon N. Y. 141 (2019) 400–416, https://doi.org/10.1016/j.carbon.2018.09.067.
[20] Z. Li, Y. Huang, L. Yuan, Z. Hao, Y. Huang, Status and prospects in sulfur-carbon composites as cathode materials for rechargeable lithium-sulfur batteries, Carbon N. Y. 92 (2015) 41–63, https://doi.org/10.1016/j.carbon.2015.03.008.
[21] S. Dörfler, M. Hagen, H. Althues, J. Tübke, S. Kaskel, M.J. Hoffmann, High capacity vertical aligned carbon nanotube/sulfur composite cathodes for

lithium–sulfur batteries, Chem. Commun. 48 (2012) 4097–4099, https://doi.org/10.1039/c2cc17925c.
[22] M. Hagen, S. Dörfler, H. Althues, J. Tübke, M.J. Hoffmann, S. Kaskel, K. Pinkwart, Lithium-sulphur batteries - binder free carbon nanotubes electrode examined with various electrolytes, J. Power Sources 213 (2012) 239–248, https://doi.org/10.1016/j.jpowsour.2012.04.004.
[23] A. Ghosh, S. Shukla, G.S. Khosla, B. Lochab, S. Mitra, Sustainable sulfur-rich copolymer/graphene composite as lithium-sulfur battery cathode with excellent electrochemical performance, Sci. Rep. 6 (2016) 1–13, https://doi.org/10.1038/srep25207.
[24] H. Li, X. Yang, X. Wang, M. Liu, F. Ye, J. Wang, Y. Qiu, W. Li, Y. Zhang, Dense integration of graphene and sulfur through the soft approach for compact lithium/sulfur battery cathode, Nano Energy 12 (2015) 468–475, https://doi.org/10.1016/j.nanoen.2015.01.007.
[25] Y. Yan, J.C. Xie, Y. Zhao, Y. Zhang, N. Cui, C. Li, C. Hao, Ionic liquid-assisted pickering emulsion synthesis of hierarchical porous carbon wrapped graphene nanosheets for high performance lithium-sulfur batteries, J. Alloys Compd. 805 (2019) 733–739, https://doi.org/10.1016/j.jallcom.2019.07.143.
[26] X.Q. Zhang, B. He, W.C. Li, A.H. Lu, Hollow carbon nanofibers with dynamic adjustable pore sizes and closed ends as hosts for high-rate lithium-sulfur battery cathodes, Nano Res. 11 (2018) 1238–1246, https://doi.org/10.1007/s12274-017-1737-6.
[27] B. He, W.C. Li, C. Yang, S.Q. Wang, A.H. Lu, Incorporating sulfur inside the pores of carbons for advanced lithium-sulfur batteries: an electrolysis approach, ACS Nano 10 (2016) 1633–1639, https://doi.org/10.1021/acsnano.5b07340.
[28] Y. Zhang, X. Zong, L. Zhan, X. Yu, J. Gao, C. Xun, P. Li, Y. Wang, Double-shelled hollow carbon sphere with microporous outer shell towards high performance lithium-sulfur battery, Electrochim. Acta 284 (2018) 89–97, https://doi.org/10.1016/j.electacta.2018.05.144.
[29] J.T. Lee, Y. Zhao, H. Kim, W. Il Cho, G. Yushin, Sulfur infiltrated activated carbon cathodes for lithium sulfur cells: the combined effects of pore size distribution and electrolyte molarity, J. Power Sources 248 (2014) 752–761, https://doi.org/10.1016/j.jpowsour.2013.10.003.
[30] R. Elazari, G. Salitra, A. Garsuch, A. Panchenko, D. Aurbach, Sulfur-impregnated activated carbon fiber cloth as a binder-free cathode for rechargeable Li-S batteries, Adv. Mater. 23 (2011) 5641–5644, https://doi.org/10.1002/adma.201103274.
[31] F.F. Zhang, X.B. Zhang, Y.H. Dong, L.M. Wang, Facile and effective synthesis of reduced graphene oxide encapsulated sulfur via oil/water system for high performance lithium sulfur cells, J. Mater. Chem. 22 (2012) 11452–11454, https://doi.org/10.1039/c2jm16543k.
[32] Z. Li, T. Huang, W. Gao, Z. Xu, D. Chang, C. Zhang, C. Gao, Hydrothermally activated graphene fiber fabrics for textile electrodes of supercapacitors, ACS Nano 11 (2017) 11056–11065, https://doi.org/10.1021/acsnano.7b05092.
[33] M.-S. Song, S.-C. Han, H.-S. Kim, J.-H. Kim, K.-T. Kim, Y.-M. Kang, H.-J. Ahn, S.X. Dou, J.-Y. Lee, Effects of nanosized adsorbing material on electrochemical properties of sulfur cathodes for Li/S secondary batteries, J. Electrochem. Soc. 151 (2004) A791, https://doi.org/10.1149/1.1710895.
[34] C. Hernández-Rentero, R. Córdoba, N. Moreno, A. Caballero, J. Morales, M. Olivares-Marín, V. Gómez-Serrano, Low-cost disordered carbons for Li/S batteries: a high-performance carbon with dual porosity derived from cherry pits, Nano Res. 11 (2018) 89–100, https://doi.org/10.1007/s12274-017-1608-1.
[35] G. Li, J. Sun, W. Hou, S. Jiang, Y. Huang, J. Geng, Three-dimensional porous carbon composites containing high sulfur nanoparticle content for high-performance lithium-sulfur batteries, Nat. Commun. 7 (2016), https://doi.org/10.1038/ncomms10601.
[36] Y.S. Su, A. Manthiram, A facile in situ sulfur deposition route to obtain carbon-wrapped sulfur composite cathodes for lithium-sulfur batteries, Electrochim. Acta 77 (2012) 272–278, https://doi.org/10.1016/j.electacta.2012.06.002.
[37] C. Luo, W. Lv, Y. Deng, G. Zhou, Z.Z. Pan, S. Niu, B. Li, F. Kang, Q.H. Yang, A dual-function Na2SO4 template directed formation of cathode materials with a high content of sulfur nanodots for Lithium–Sulfur batteries, Small 13 (2017) 1–7, https://doi.org/10.1002/smll.201700358.
[38] R. Fang, C. Liang, Y. Xia, Z. Xiao, H. Huang, Y. Gan, J. Zhang, X. Tao, W. Zhang, Supercritical CO_2 mediated incorporation of sulfur into carbon matrix as cathode materials towards high-performance lithium-sulfur batteries, J. Mater. Chem. A. 6 (2017) 212–222, https://doi.org/10.1039/c7ta08768c.
[39] A. Baklavaridis, I. Zuburtikudis, C. Panayiotou, Nanofibrous morphology of electrospun chitosan nanocomposites reinforced with WS_2 nanotubes: a design-of-experiments study, J. Ind. Text. 48 (2018) 119–145, https://doi.org/10.1177/1528083717725114.
[40] M.A. Pigaleva, I.V. Elmanovich, M.N. Temnikov, M.O. Gallyamov, A.M. Muzafarov, Organosilicon compounds in supercritical carbon dioxide: synthesis, polymerization, modification, and production of new materials, Polym. Sci. - Ser. B. 58 (2016) 235–270, https://doi.org/10.1134/S1560090416030118.
[41] P.B. Arthi G, L. BD, A simple approach to stepwise synthesis of graphene oxide nanomaterial, J. Nanomed. Nanotechnol. 6 (2015) 1–4, https://doi.org/10.4172/2157-7439.1000253.
[42] S.N. Alam, N. Sharma, L. Kumar, Synthesis of graphene oxide (GO) by modified hummers method and its thermal reduction to obtain reduced graphene oxide (rGO), Graphene 6 (2017) 1–18, https://doi.org/10.4236/graphene.2017.61001.
[43] S. Pei, H.M. Cheng, The reduction of graphene oxide, Carbon N. Y. 50 (2012) 3210–3228, https://doi.org/10.1016/j.carbon.2011.11.010.
[44] H. Ham, T. Van Khai, N.H. Park, D.S. So, J.W. Lee, H.G. Na, Y.J. Kwon, H.Y. Cho, H.W. Kim, Freeze-drying-induced changes in the properties of graphene oxides, Nanotechnology 25 (2014), https://doi.org/10.1088/0957-4484/25/23/235601.
[45] J. Zhao, L. Zhang, X. Li, X. Tao, W. Zhu, X. Ye, Supercritical CO_2 assisted fabrication of activated carbon-sulfur composite for improved lithium-sulfur batteries, J. Alloys Compd. 708 (2017) 264–269, https://doi.org/10.1016/j.jallcom.2017.02.289.
[46] L. Stobinski, B. Lesiak, J. Zemek, P. Jiricek, Time dependent thermal treatment of oxidized MWCNTs studied by the electron and mass spectroscopy methods, Appl. Surf. Sci. 258 (2012) 7912–7917, https://doi.org/10.1016/j.apsusc.2012.04.127.
[47] Y. Yamada, H. Yasuda, K. Murota, M. Nakamura, T. Sodesawa, S. Sato, Analysis of heat-treated graphite oxide by X-ray photoelectron spectroscopy, J. Mater. Sci. 48 (2013) 8171–8198, https://doi.org/10.1007/s10853-013-7630-0.
[48] A.V. Naumkin, A. Kraut-Vass, S.W. Gaarenstroom, C.J. Powell, NIST X-Ray Photoelectron Spectroscopy Database, 2003, https://doi.org/10.18434/T4T88K, Version 3.4.
[49] B.A. Boukamp, Fourier transform distribution function of relaxation times; application and limitations, Electrochim. Acta 154 (2015) 35–46, https://doi.org/10.1016/j.electacta.2014.12.059.
[50] F. Ciucci, C. Chen, Analysis of electrochemical impedance spectroscopy data using the distribution of relaxation times: a Bayesian and hierarchical Bayesian approach, Electrochim. Acta 167 (2015) 439–454, https://doi.org/10.1016/j.electacta.2015.03.123.
[51] M.B. Effat, F. Ciucci, Bayesian and hierarchical bayesian based regularization for deconvolving the distribution of relaxation times from electrochemical impedance spectroscopy data, Electrochim. Acta 247 (2017) 1117–1129, https://doi.org/10.1016/j.electacta.2017.07.050.
[52] J. Liu, T.H. Wan, F. Ciucci, A Bayesian view on the Hilbert transform and the Kramers-Kronig transform of electrochemical impedance data: probabilistic estimates and quality scores, Electrochim. Acta 357 (2020), 136864, https://doi.org/10.1016/j.electacta.2020.136864.
[53] M. Saccoccio, T.H. Wan, C. Chen, F. Ciucci, Optimal regularization in distribution of relaxation times applied to electrochemical impedance spectroscopy: Ridge and Lasso regression methods - a theoretical and experimental Study, Electrochim. Acta 147 (2014) 470–482, https://doi.org/10.1016/j.electacta.2014.09.058.
[54] A.N. Tikhonov, V.J. Arsenin, Solutions of Ill-Posed Problems, Halsted Press Books, 1977.
[55] A.L. Gavrilyuk, D.A. Osinkin, D.I. Bronin, The use of Tikhonov regularization method for calculating the distribution function of relaxation times in impedance spectroscopy, Russ. J. Electrochem. 53 (2017) 575–588, https://doi.org/10.1134/S1023193517060040.
[56] T. Paul, P.W. Chi, P.M. Wu, M.K. Wu, Computation of distribution of relaxation times by Tikhonov regularization for Li ion batteries: usage of L-curve method, Sci. Rep. 11 (2021) 1–9, https://doi.org/10.1038/s41598-021-91871-3.
[57] J. Landesfeind, J. Hattendorff, A. Ehrl, W.A. Wall, H.A. Gasteiger, Tortuosity determination of battery electrodes and separators by impedance spectroscopy, J. Electrochem. Soc. 163 (2016) A1373, https://doi.org/10.1149/2.1141607jes. –A1387.
[58] Z. Wang, Y. Dong, H. Li, Z. Zhao, H. Bin Wu, C. Hao, S. Liu, J. Qiu, X.W.D. Lou, Enhancing lithium-sulphur battery performance by strongly binding the discharge products on amino-functionalized reduced graphene oxide, Nat. Commun. 5 (2014), https://doi.org/10.1038/ncomms6002.
[59] R. Pongilat, S. Franger, K. Nallathamby, Functionalized carbon as polysulfide traps for advanced lithium-sulfur batteries, J. Phys. Chem. C 122 (2018) 5948–5955, https://doi.org/10.1021/acs.jpcc.8b00605.
[60] P.J.H. Kim, K. Kim, V.G. Pol, Towards highly stable lithium sulfur batteries: surface functionalization of carbon nanotube scaffold, Carbon N. Y. 131 (2018) 175–183, https://doi.org/10.1016/j.carbon.2018.01.100.
[61] Z. Sun, J. Zhang, L. Yin, G. Hu, R. Fang, H.M. Cheng, F. Li, Conductive porous vanadium nitride/graphene composite as chemical anchor of polysulfides for lithium-sulfur batteries, Nat. Commun. 8 (2017), https://doi.org/10.1038/ncomms14627.
[62] D. Liu, C. Zhang, G. Zhou, W. Lv, G. Ling, L. Zhi, Q.H. Yang, Catalytic effects in Lithium–Sulfur batteries: promoted sulfur transformation and reduced shuttle effect, Adv. Sci. 5 (2018), https://doi.org/10.1002/advs.201700270.
[63] C. Zheng, S. Niu, W. Lv, G. Zhou, J. Li, S. Fan, Y. Deng, Z. Pan, B. Li, F. Kang, Q.H. Yang, Propelling polysulfides transformation for high–rate and long-life lithium–sulfur batteries, Nano Energy 33 (2017) 306–312, https://doi.org/10.1016/j.nanoen.2017.01.040.
[81] N. Jayaprakash, J. Shen, S.,M. Surya, A. Corona, A.A. Lynden, Porous hollow Carbon@Sulfur composites for High–Power lithium–sulfur batteries, Angew. Chem. Int. Ed. 50 (2011) 5904–5908, https://doi.org/10.1002/anie.201100637.
[82] Y. Guang, T. Runming, J.,J. Charl, S. Chao, Z. Sheng, H. Lilin, B. Ilias, N. Jagjit, Investigating multiscale spatial distribution of sulfur in a CNT scaffold and its impact on Li–S cell performance, J. Phys. Chem. C 125 (2021) 13146–13157, https://doi.org/10.1021/acs.jpcc.1c02288.
[83] W. Feixiang, T.,L. Jung, Z. Enbo, Z. Bao, Yu Gleb, Graphene–Li2S–Carbon nanocomposite for Lithium–Sulfur batteries, ACS Nano 10 (2016) 1333–1340, https://doi.org/10.1021/acsnano.5b06716.

[84] B. Zhang, X. Qin, G.,R. Lia, X.,P. Gao, Enhancement of long stability of sulfur cathode by encapsulating sulfur into micropores of carbon spheres, Energy Environ. Sci. 3 (2010) 1531−1537, https://doi.org/10.1039/c002639e.

[85] J. Wang, Y. Liu, M. Cheng, H. Zhao, J. Wang, J. Zhao, X. Duan, C. Wang, J. Wang, Hierarchical porous carbon-graphene-based Lithium Sulfur batteries, Electrochim. Acta 318 (2019) 161−168, https://doi.org/10.1016/j.electacta.2019.05.090.